ARTICLE

Graphene Nanomesh by ZnO Nanorod Photocatalysts

Omid Akhavan*

Department of Physics, Sharif University of Technology, P.O. Box 11155-9161, Tehran, Iran, and Institute for Nanoscience and Nanotechnology, Sharif University of Technology, P.O. Box 14588-89694, Tehran, Iran

ABSTRACT Local photodegradation of graphene oxide sheets at the tip of ZnO nanorods was used to achieve semiconducting graphene nanomeshes. The chemically exfoliated graphene oxide sheets, with a thickness of ~0.9 nm, were deposited on quartz substrates. Vertically aligned ZnO nanorod arrays with diameters of 140 nm and lengths of <1 μm were grown on a glass substrate by using a hydrothermal method. The graphene oxide sheets were physically attached to the tip of the ZnO nanorods by assembling the sheets on the nanorods. UV-assisted photodegradation of the graphene oxide sheets (with dimension of ~5 × 5 μm) at a contact place with the ZnO nanorods resulted in graphene nanomeshes with a pore size of ~200 nm. The graphene nanomeshes prepared by using the photocatalytic property of the ZnO nanorods contained smaller oxygen-containing carbonaceous bonds and higher defects as compared to the as-prepared graphene oxide sheets. When chemical reduction of the graphene nanomeshes by hydrazine was used, the oxygen bonds of the nanomeshes more decreased while their graphitization increased. Based on X-ray photoelectron spectroscopy at low binding energies, the graphene nanomeshes reduced by hydrazine exhibited as a broad sheet a p-type semiconductor with an ~1.2 eV energy gap between the valence band and the Fermi level.

KEYWORDS: carbon nanostructures · graphene · ZnO nanorods · photocatalysis · semiconductor

Among various carbon nanostructures, graphene as a single-atom-thick sheet arranged by sp^2-bonded carbon atoms in a hexagonal lattice shows unique properties for both fundamental research[1−4] and promising applications in condensed-matter physics, electronics, and material science.[5−13] The interest to the graphene-based subjects has been extremely increased after empirical discovery of graphene sheets in 2004.[14]

Graphene as a two-dimensional transparent conductor with excellent mobility (~15000 $m^2V^{-1}s^{-1}$ at room temperature) is considered as a highly promising candidate for developing electronics.[14−17] However, graphene with a zero band gap cannot be applied in field-effect transistors working at room temperature.[1,18] This problem could be eliminated by transforming graphene sheets into nanoribbons with widths of <10 nm, because such nanoribbons show a semiconductor behavior with a band gap suitable for transistor operation at room temperature.[19−30] But, in addition to the hard production of high quality nanoribbons, they often show low driving currents or transconductances as important challenges.[29,30] Therefore, other methods should be considered to overcome such problems. For example, modulation of electrical properties and the band gap structure of N-doped graphene as an n-type semiconductor were studied by Wei et al.[31] Band-gap adjustment of graphene by adsorption of molecules on its surface was also proposed.[32] Recently, Bai et al.[33] reported a new graphene nanostructure as a "graphene nanomesh" that can open up a band gap in a large sheet of graphene to create a p-type semiconducting thin film. To produce the graphene nanomesh, they used a block copolymer lithography method. It was recently shown that, as the flash energy can reduce the graphene oxide sheets, it can also be used for patterning the reduced sheets.[34] Therefore, the photoreduction procedures may be applied as both reducing and patterning tools. In fact, it was recently reported that graphene oxides can chemically interact with TiO_2 nanoparticles and thin films in a photocatalytic reduction process.[35,36] In addition, it was shown that carbon bonds of graphene can be cut by oxidation.[37] Because oxidation and decomposition of carbonaceous materials, using metal oxide semiconductor photocatalysts, such as TiO_2 and ZnO, are well-known,[38,39] local photodegradation of graphene sheets by the nanostructured

*Address correspondence to oakhavan@sharif.edu.

Received for review April 11, 2010 and accepted June 7, 2010.

Published online June 15, 2010.
10.1021/nn1007429

photocatalysts can be nominated as one of the ways to produce graphene nanomeshes.

In this work, formation of graphene nanomeshes by using local photodegradation of chemically synthesized graphene oxide sheets at the contact place of the tip of vertically aligned ZnO nanorods was investigated. The surface topography of the graphene nanomeshes was studied by atomic force microscopy (AFM). Furthermore, the carbon structure and chemical state of the synthesized graphene oxide sheets and graphene nanomeshes were investigated and compared by Raman and X-ray photoelectron spectroscopy (XPS). The electronic structure of the graphene nanomeshes, as semiconductors, was examined by XPS analysis at low binding energies.

RESULTS AND DISCUSSION

Surface morphology of the vertically aligned ZnO nanorods has been presented in Figure 1. It is seen that the ZnO nanorods were grown uniformly on the ZnO seed layer in a densely packed structure. To better observe the morphology of the ZnO nanorods (especially the morphology of the tip of the nanorods), TEM was utilized, as is also shown in Figure 1. The diameter of the ZnO nanorods was about 140 nm, and their average length was less than ~1 μm. Such morphologies were also previously reported for the ZnO nanorods prepared by a hydrothermal method.[40] Some additional details about the ZnO nanorods synthesized by the hydrothermal method can also be found elsewhere.[41]

To characterize the surface topography of the graphene sheets, AFM was utilized as an appropriate technique. Figure 2 shows AFM images of the as-prepared graphene oxide sheets (Figure 2a) and the graphene nanomesh (Figure 2b). They present some partially overlapped sheets deposited on the quartz substrate. In Figure 2a, the height profile diagram shows that the thickness of the sheets was ~0.9 nm, in good agreement with the typical thickness of the single-layer graphene oxides, that is, ~0.8 nm.[42] In fact, due to the presence of epoxy and hydroxyl bonds on both sides of the graphene oxide sheets, the typical thickness of the oxide sheets is at least ~0.44 nm greater than the thickness of graphene (~0.36 nm).[42,43] Therefore, our AFM analysis showed that the as-prepared samples contained single-layer graphene oxide sheets partially overlapped on each other (see also the Raman analysis). Figure 2 shows the same sheets after the photocatalytic process of the graphene oxide sheets assembled on the vertically aligned ZnO nanorods. Some pores are clearly seen on the sheets, indicating formation of porous sheets after the photocatalytic process. The pores can be assigned to the photodegradation trace of the tip of the ZnO nanorods attached to the surface of the sheets. The height profile diagram of the AFM image of the porous sheets shows that

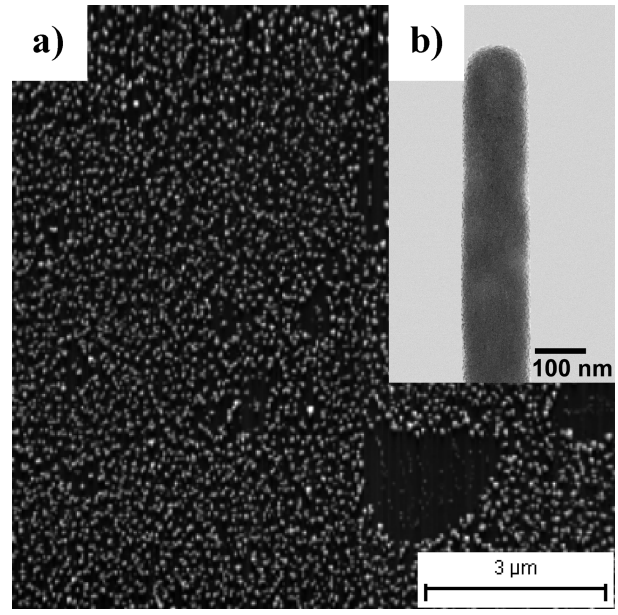

Figure 1. (a) SEM image of vertically aligned ZnO nanorods grown on the ZnO seed layer and (b) TEM image of one of the ZnO nanorods.

thickness of the oversheets (~0.5 nm) were smaller than the typical thickness of the graphene oxide layer (~0.8 nm). This decrease in the thickness can be attributed to partial reduction of the graphene oxide sheets during the photocatalytic process by the ZnO nanorod photocatalysts (see also the XPS results). In addition, thickness of the underneath sheets (~0.8 nm) was slightly decreased as compared to the thickness of the sheets in the as-prepared samples (~0.9 nm). The depth of the pores in the height profile diagram indicates complete photodegradation of the graphene oxide sheets at the contact place of the tip of the nanorods with the sheets. Typical diameter of the pores was estimated around 200 nm, which is greater than the typical diameter of the ZnO nanorods. This indicates extension of the photodegradation process out of the contact place of the tip of the ZnO nanorods with the sheets.

The chemically exfoliated graphene oxides include a variety of functional groups such as hydroxyl (C−OH) and epoxide (C−O−C) groups in addition to carbonyl (>C═O) and carboxyl (−COOH) groups usually present at the defects and edges of the sheets. To investigate the chemical state of the graphene oxide sheets and graphene nanomeshes, XPS was utilized. The deconvoluted C(1s) XPS core levels of the graphene oxide sheets and graphene nanomeshes deposited on the quartz substrate have been presented in Figure 3. The deconvoluted peak located at the binding energy of 285.0 eV was attributed to the C−C, C═C, and C−H bonds. The deconvoluted peaks centered at the binding energies of 286.0, 287.5, and 289.5 eV were assigned to the C−OH, C═O, and O═C−OH oxygen-containing carbonaceous bands, respectively.[36,44−46] In the most

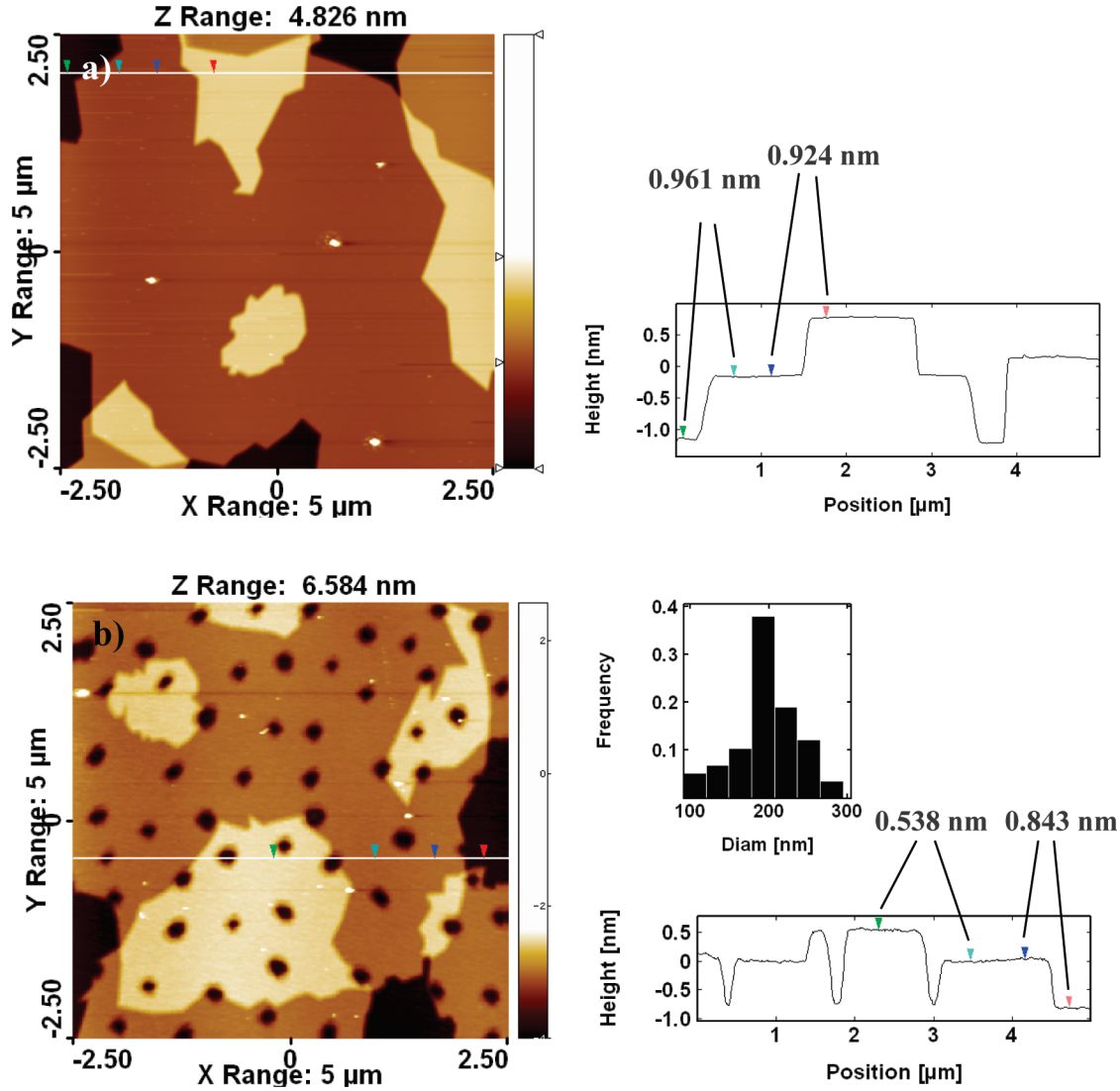

Figure 2. AFM images of (a) the graphene oxide sheets and (b) the graphene nanomeshes on quartz substrates. In the height profile diagrams, vertical distances of each couple marker have been mentioned above them. The diameter histogram of the pores shown in image (b) was also presented.

structural models of graphite oxides, the hydroxyl and epoxide groups show similar C(1s) binding energies.[47] Hence, the contribution of epoxide and hydroxyl groups was not separated in the deconvoluted C(1s) core level. For the as-prepared graphene oxide sheets (Figure 3a), considerable amounts of the oxygen-containing carbonaceous bands were detected in the deconvoluted carbon peak, as expected. For assigning comparative values to the amount of the oxygen-containing carbonaceous bands, the peak area ratios of the C−OH, C═O, and O═C−OH bonds to the CC bonds (containing C−C, C═C, and C−H bonds) were calculated and also presented in Table 1. The XPS analysis (Figure 3b) showed that the oxygen-containing carbonaceous bond ratios of the C−OH, C═O, and O═C−OH bonds of the graphene nanomeshes decreased 63, 33, and 55% relative to the corresponding bonds on the as-prepared graphene oxide sheets, re-

TABLE 1. Peak Area (*A*) Ratios of the Oxygen-Containing Bonds to the CC Bonds and the Total Carbon Bands to the Si Band of the Quartz Substrate (by XPS), and the Peak Intensity Ratios of I_D/I_G (by Raman Analysis) of the Graphene Oxide Sheets, Graphene Nanomeshes, and Graphene Nanomeshes Reduced by Hydrazine

	XPS				Raman
sample	A_{COH}/A_{CC}	A_{CO}/A_{CC}	A_{OCOH}/A_{CC}	normalized $(A_C/A_{Si})^a$	I_D/I_G
graphene oxide	0.74	1.13	0.18	1	1.00
graphene nanomesh	0.27	0.75	0.08	0.69	1.33
graphene nanomesh reduced by N_2H_4	0.20	0.44	0.06	0.71	1.17

$^a A_C = A_{CC} + A_{COH} + A_{CO} + A_{OCOH}$.

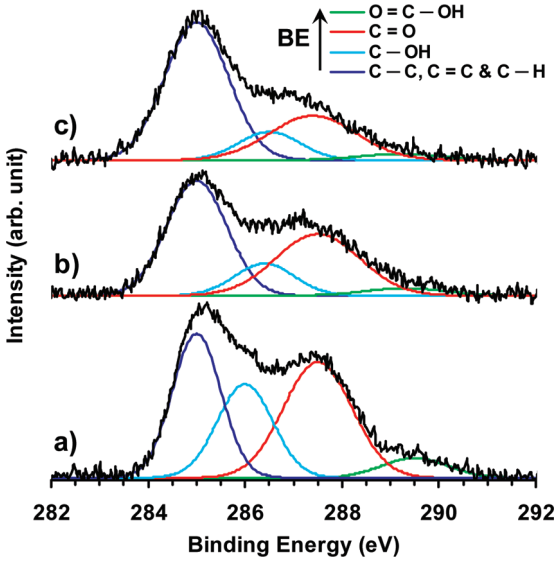

Figure 3. Peak deconvolution of C(1s) XPS core level of (a) the graphene oxide sheets, (b) the graphene nanomeshes, and (c) the graphene nanomeshes reduced by hydrazine.

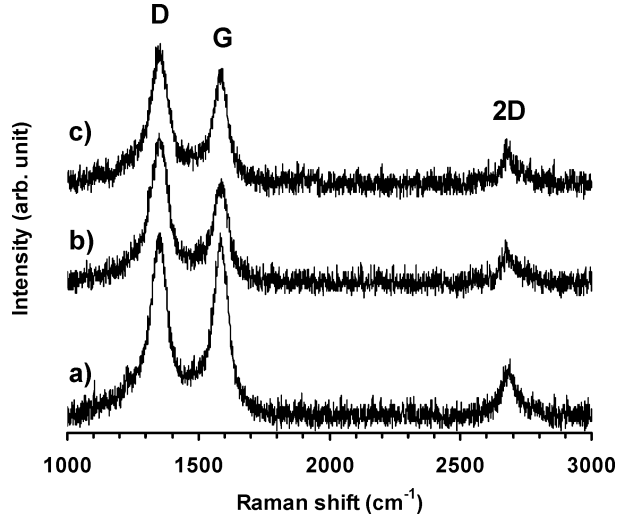

Figure 4. Raman spectra of (a) the graphene oxide sheets, (b) the graphene nanomeshes, and (c) the graphene nanomeshes reduced by hydrazine.

spectively. This means partial chemical reduction of the graphene oxide sheets during the photocatalytic reduction by the ZnO nanorods. In fact, photocatalytic reduction of graphene oxides was previously reported.[35,36] For example, the XPS analysis of graphene oxide/TiO_2 thin film showed that the photocatalytic reduction can reduce the C−OH, C═O, and O═C−OH band ratios down to 73, 85, and 72%, respectively.[36] The weaker photocatalytic reduction of the graphene oxide sheets in this work can be assigned to the smaller and local contact area between the photocatalyst and the graphene oxide sheets. In addition, formation of pores in the graphene oxide sheets (as defects) prevented substantial reduction of the oxygen-containing carbonaceous bonds, particularly the C═O bond at the edges of pores. To better reduce the obtained graphene nanomeshes, they were reduced by hydrazine. The deconvoluted C(1s) XPS core levels of the graphene nanomeshes reduced by hydrazine presented in Figure 3c showed that hydrazine could further reduce the graphene nanomeshes (see also Table 1). Based on the decrease in the peak area ratio of the C(1s) to Si(2p) core levels (A_C/A_{Si}), it was found that the carbon content of the graphene nanomeshes also decreased about 30% relative to the corresponding value in the graphene oxide sheets. The decrease in carbon content of the sheets is completely consistent with the photodegradation process, which caused the pores in the sheets.

Raman spectroscopy was used to study the ordered/disordered crystal structures of carbonaceous materials. Thus, we utilized it to examine the changes that occurred in the structure of the graphene nanomeshes as compared to the as-prepared graphene oxide sheets, as shown in Figure 4. The well-known characteristics of carbon materials in Raman spectra are the G band (~1580 cm^{-1}), which is generally assigned to the E_{2g} phonon of sp^2 bonds of carbon atoms, and the D band (~1350 cm^{-1}) as a breathing mode of κ-point phonons of A_{1g} symmetry,[48,49] which is attributed to local defects and disorders, particularly the defects located at the edges of graphene and graphite platelets.[50] Hence, the smaller I_D/I_G peak intensity ratio of a Raman spectrum can indicate lower defects and disorders of the graphitized structures containing the disorders caused at the edges of the carbon platelets. The Raman spectra shown in Figure 4 display the D and G bands at about 1348 and 1583 cm^{-1}, respectively. It was also found that the I_D/I_G ratio increased from 1.00 for the graphene oxide sheets to 1.33 for the graphene nanomeshes. This increase was assigned to formation of the pores (as defects and disorders) in the graphene sheets. By reducing the graphene nanomeshes by hydrazine, the I_D/I_G ratio decreased to 1.17, which can be assigned to more graphitization of the nanomeshes due the reduction process.

Raman spectroscopy is also utilized to investigate the single-, bi-, and multilayer characteristics of graphene and graphene oxide layers. For instance, it was shown that the G band of the single-layer graphene, located at 1585 cm^{-1}, shifts about 6 cm^{-1} into lower wavenumbers after stacking 2−6 graphene layers.[43,50−53] Moreover, the shape and position of the 2D band are known as key parameters to judge both formation and the layer numbers of the graphene sheets.[43,51−54] The 2D band of the single-layer graphene sheets is usually observed at 2679 cm^{-1}, while for the multilayers (2−4 layers) it shifts to higher wavenumbers by 19 cm^{-1}.[50] In this work, the slight shift of the peak position of the G band to lower wavenumbers (2 cm^{-1} shift) can be assigned to the presence of both single- and multilayer graphene oxide sheets in the deposited samples. For the graphene oxide sheets,

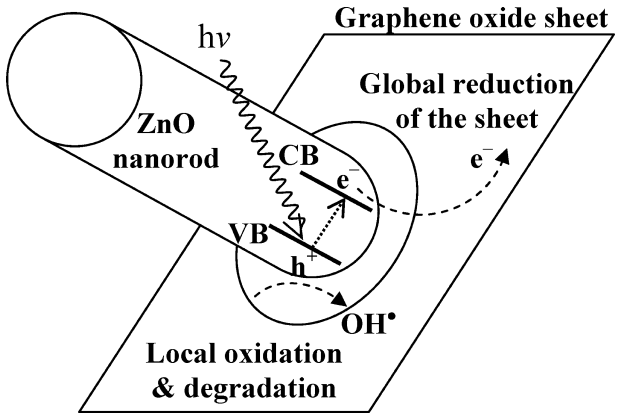

Figure 5. Schematic illustration of the mechanism describing formation of graphene nanomeshes by using the photocatalytic property of the ZnO nanorods.

peak position of the 2D band at 2683 cm^{-1} and the nearly asymmetrical shape of the peak also confirmed the presence of both single- and multilayer graphene oxide sheets in the deposited samples. For the graphene nanomeshes, the asymmetrical shape of the 2D band is clearly seen, showing the presence of the multilayer graphene nanomesh in the samples. On the other hand, the slight peak position shift of the 2D band (~10 cm^{-1}) into the lower wavenumbers indicated more contribution of single-layer sheets in the porous graphene sample. This can be attributed to removing some surface carbon layers due to the photodegradation process. No considerable change in the 2D band was observed after reduction of the graphene nanomeshes.

Formation of the graphene nanomeshes by using the ZnO nanorods in a photodegradation process can be explained based on the following proposed mechanism. Concerning this, a schematic illustration was also presented in Figure 5. Under UV irradiation, the photoexcited electrons were injected from the tip of the ZnO nanorods into the graphene oxide sheets, because graphene oxide sheets are known as good electron acceptors. Due to high mobility of the electrons in the graphene sheets, the injected electrons can easily move throughout each sheet and can reduce it globally (even far from the contact place of the ZnO nanorods with the sheet). It was previously shown that the synthesized ZnO nanorods possessed a considerable amount of hydroxyl groups on their surfaces and that they exhibited a hydrophilic property.[41] Thus, the holes accumulated in the tip of the excited ZnO nanorods could effectively produce active $OH^{\bullet}$ radicals near the surface of the tip for the local oxidation and, subsequently, the local degradation of the sheets. The larger diameter of the pores, as compared to the diameter of the nanorods, can be assigned to higher humidity near the hydrophilic tip of the nanorods, that is, around the contact place of the nanorods with the sheets.

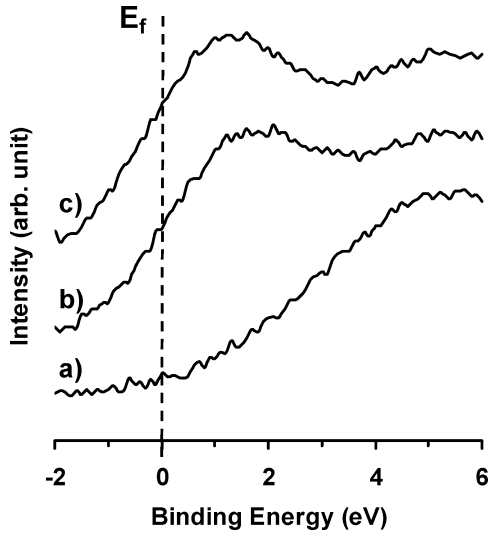

Figure 6. XPS valence spectra of (a) the graphene oxide sheets, (b) the graphene nanomeshes, and (c) the graphene nanomeshes reduced by hydrazine.

Some electrical characteristics of the graphene oxide sheets and the graphene nanomeshes can also be examined by using XPS. In fact, XPS analysis at low binding energies can determine the electron density of the valence band on the surface of the films, as previously reported for graphene-[55] and silicide-based materials.[56] Figure 6 presents XPS spectra of the graphene nanomeshes, as compared to the spectrum of the graphene oxide sheets. For the graphene oxide sheets, the valence band was found to be very far from the Fermi level (E_f). In contrast, for the graphene nanomeshes and the graphene nanomeshes reduced by hydrazine, the nearest peaks to the Fermi level were found at binding energies of ~1.6 and 1.2 eV, respectively. Because the valence band of the graphene nanomeshes before and after reduction by hydrazine was not changed substantially, the valence band approaching the graphene oxide sheets into the Fermi level after the photocatalytic process can be mainly attributed to the reduction of the graphene oxide sheets. In addition, reduction of the graphene nanomeshes by hydrazine could not reduce the distance of the valence band peak to zero. In fact, the graphene nanomeshes (even after reduction by hydrazine) exhibited a p-type semiconducting behavior, similar to the results recently reported by Bai et al.[33] It was previously shown that the valence band peak of graphene oxide sheets reduced by thermal reduction coincided on the Fermi level, indicating an electrical conducting behavior.[55] Here, the synthesized graphene nanomeshes presented a semiconducting behavior in a relatively broad sheet (~5 × 5 μm), without any doping.

CONCLUSIONS

Graphene nanomeshes were synthesized using local photodegradation of graphene oxide sheets by the tip of vertically aligned ZnO nanorod arrays. AFM images illustrated formation of the graphene nanomeshes with a pore size of about 200 nm. The

XPS and Raman spectra showed that the graphene nanomeshes contained smaller oxygen-containing carbonaceous bonds and higher carbon defects as compared to the as-prepared graphene oxide sheets. This indicated partial photocatalytic reduction of the graphene oxides during the local photodegradation of graphene sheets at the contact place with the tip of the ZnO nanorods, because a better chemical reduction was obtained by using hydrazine. Both Raman and AFM analyses confirmed the presence of single-layer graphene oxide sheets in addition to the presence of some multilayer ones. The graphene nanomeshes presented a p-type semiconducting behavior in a wide sheet and with no doping. Hence, the synthesized graphene nanomeshes can be considered one of the important nanomaterials in future graphene-based research and technologies.

EXPERIMENTAL SECTION

Synthesis of Graphene Oxide Sheets. The improved Hummers method[5,57] was utilized to oxidize natural graphite powder (particle diameter of 45 μm, Sigma-Aldrich). In a typical method, 50 mL of H_2SO_4 was added into a flask containing 2 g graphite at room temperature. The flask was cooled to 0 °C in an ice bath. Then, 6 g potassium permanganate ($KMnO_4$) was added slowly to the above mixture and left to warm to room temperature. The suspension was stirred continuously for 2 h at 35 °C. Then, it was cooled in an ice bath and, subsequently, diluted with 350 mL of deionized (DI) water. H_2O_2 (30%) was then added to reduce the residual permanganate to soluble manganese ions: the state in which the gas evolution was stopped. Eventually, the resulting suspension was filtered, washed with 1 M HCl and several times with DI water, and dried at 60 °C for 24 h to obtain a brownish graphite oxide powder. The obtained graphite oxide powder was dispersed in water (1 mg/mL) to obtain a suspension. Then the suspension was sonicated for 30 min to obtain a graphene oxide suspension.

Growth of ZnO Nanorods. To prepare ZnO nanorods, at first a ZnO seed layer was prepared using zinc acetate solution. The required solutions were prepared by dissolving zinc acetate ($Zn(CH_3COO_2)\cdot 2H_2O$) into ethanol (0.5 mol/L) and then adding diethanolamine (DEA) in the solution. The molar ratio of DEA to zinc acetate was 6:5. Then, the obtained solution was stirred at 60 °C for 30 min to achieve a clear and homogeneous soln. The ZnO seed layers were obtained by dipping glass substrates in the prepared soln for 2 min at room temperature and pulling up vertically at a speed of about 30 mm/min. After drying the films at room temperature in air for 1 h, they were annealed at 400 °C in air for 1 h. The dip-coating and the subsequent annealing process were performed two times to obtain a thicker and more uniform ZnO seed layer.

A hydrothermal process was used for growth of free-catalyst ZnO nanorods on the seed layers. After washing the ZnO seed layers with deionized (DI) water, they were suspended in a supersaturated aqueous solution of 0.001 M $Zn(NO_3)_2$/0.05 M NaOH, while the solution was stirred at 70 °C for 2 h. Finally, the resultant samples containing the ZnO nanorods were rinsed with DI water and dried at room temperature.

Producing Graphene Nanomesh by ZnO Nanorod Photocatalysts. The graphene oxide sheets were deposited on quartz substrate by drop-casting the graphene oxide suspension onto the substrate cleaned by DI water, methanol, and UV irradiation for 2 h. The samples were dried at 100 °C in air for 30 min. Then the graphene oxide sheets were assembled on the vertically aligned ZnO nanorods so that the tip of the ZnO nanorods could make contact with the graphene oxide sheets. This structure was illuminated by a UV-LED source with 5 mW/cm^2 intensity and a wavelength peak at 255 nm for 10 h. Some of the obtained graphene nanomesh samples were also reduced by a hydrazine vapor for 1 h.

Material Characterization. Surface morphology of the ZnO nanorods was studied by using a Philips XL30 scanning electron microscope (SEM). A Philips-CM200 transmission electron microscopy (TEM) apparatus operated at 200 kV was also used to better observe the morphology of the grown ZnO nanorods. For sample preparation, the ZnO film was scratched and immersed in methanol. Then, a holey copper grid was dipped in the solution for TEM imaging. AFM images of the graphene oxide sheets deposited on quartz substrates were obtained by using a Park Scientific model CP-Research (VEECO). XPS was applied to examine the carbonaceous band ratios and the chemical states of the graphene oxide sheets. The data were obtained using a hemispherical analyzer with an Al Kα X-ray source ($h\nu = 1486.6$ eV) working in a vacuum better than 10^{-7} Pa. The XPS peaks were deconvoluted using Gaussian components after a Shirley background subtraction. Raman spectroscopy was performed using a Raman Microprobe (HR-800 Jobin-Yvon) with a 532 nm Nd:YAG excitation source at room temperature.

Acknowledgment. The author would like to thank the Research Council of Sharif University of Technology and also the Iran Nanotechnology Initiative Council for the financial support of the work.

REFERENCES AND NOTES

1. Novoselov, K. S.; Geim, A. K.; Morozov, S. V.; Jiang, D.; Katsnelson, M. I.; Grigorieva, I. V.; Dubonos, S. V.; Firsov, A. A. Two-Dimensional Gas of Massless Dirac Fermions in Graphene. *Nature* **2005**, *438*, 197–200.
2. Meyer, J. C.; Geim, A. K.; Katsnelson, M. I.; Novoselov, K. S.; Booth, T. J.; Roth, S. The Structure of Suspended Graphene Sheets. *Nature* **2007**, *446*, 60–63.
3. Katsnelson, M. I.; Novoselov, K. S. Graphene: New Bridge Between Condensed Matter Physics and Quantum Electrodynamics. *Solid State Commun.* **2007**, *143*, 3–13.
4. Schedin, F.; Geim, A. K.; Morozov, S. V.; Hill, E. W.; Blake, P.; Katsnelson, M. I.; Novoselov, K. S. Detection of Individual Gas Molecules Adsorbed on Graphene. *Nat. Mater.* **2007**, *6*, 652–655.
5. Stankovich, S.; Dikin, D. A.; Piner, R. D.; Kohlhaas, K. A.; Kleinhammes, A.; Jia, Y.; Nguyen, S. T.; Ruoff, R. S. Synthesis of Graphene-Based Nanosheets via Chemical Reduction of Exfoliated Graphite Oxide. *Carbon* **2007**, *45*, 1558–1565.
6. Gomez-Navarro, C.; Weitz, R. T.; Bittner, A. M.; Scolari, M.; Mews, A.; Burghard, M.; Kern, K. Electronic Transport Properties of Individual Chemically Reduced Graphene Oxide Sheets. *Nano Lett.* **2007**, *7*, 3499–3503.
7. Gilje, S.; Han, S.; Wang, M.; Wang, K. L.; Kaner, R. B. A Chemical Route to Graphene for Device Applications. *Nano Lett.* **2007**, *7*, 3394–3398.
8. Robinson, J. T.; Perkins, F. K.; Snow, E. S.; Wei, Z. Q.; Sheehan, P. E. Reduced Graphene Oxide Molecular Sensors. *Nano Lett.* **2008**, *8*, 3137–3140.
9. Arsat, R.; Breedon, M.; Shafiei, M.; Spizziri, P. G.; Gilje, S.; Kaner, R. B.; Kalantar-zadeh, K.; Wlodarski, W. Graphene-Like Nano-Sheets for Surface Acoustic Wave Gas Sensor Applications. *Chem. Phys. Lett.* **2009**, *467*, 344–347.
10. Wang, X.; Zhi, L. J.; Tsao, N.; Tomovic, Z.; Li, J. L.; Mullen, K. Transparent Carbon Films as Electrodes in Organic Solar Cells. *Angew. Chem., Int. Ed.* **2008**, *47*, 2990–2992.
11. Liang, X.; Fu, Z.; Chou, S. Y. Graphene Transistors Fabricated via Transfer-Printing in Device Active-Areas on Large Wafer. *Nano Lett.* **2007**, *7*, 3840–3844.
12. Stampfer, C.; Schurtenberger, E.; Molitor, F.; Güttinger, J.; Ihn, T.; Ensslin, K. Tunable Graphene Single Electron Transistor. *Nano Lett.* **2008**, *8*, 2378–2383.

13. Bao, W.; Zhang, H.; Bruck, J.; Lau, C. N.; Bockrath, M.; Standley, B. Graphene-Based Atomic-Scale Switches. *Nano Lett.* **2008**, *8*, 3345–3349.
14. Novoselov, K. S.; Geim, A. K.; Morozov, S. V.; Jiang, D.; Zhang, Y.; Dubonos, S. V.; Grigorieva, I. V.; Firsov, A. A. Electric Field Effect in Atomically Thin Carbon Films. *Science* **2004**, *306*, 666–669.
15. Zhang, Y. B.; Tan, Y.; Stormer, H. L.; Kim, P. Experimental Observation of Quantum Hall Effect and Berry's Phase in Graphene. *Nature* **2005**, *438*, 201–204.
16. Scott Bunch, J.; Yaish, Y.; Brink, M.; Bolotin, K.; McEuen, P. L. Coulomb Oscillations and Hall Effect in Quasi-2D Graphite Quantum Dots. *Nano Lett.* **2005**, *5*, 287–290.
17. Geim, A. K.; Novoselov, K. S. The Rise of Graphene. *Nat. Mater.* **2007**, *6*, 183–191.
18. Meric, I.; Han, M. Y.; Young, A. F.; Ozyilmaz, B.; Kim, P.; Shepard, K. L. Current Saturation in Zero-Bandgap, Topgated Graphene Field-Effect Transistors. *Nat. Nanotechnol.* **2008**, *3*, 654–659.
19. Nakada, K.; Fujita, M.; Dresselhaus, G.; Dresselhaus, M. S. Edge State in Graphene Ribbons: Nanometer Size Effect and Edge Shape Dependence. *Phys. Rev. B* **1996**, *54*, 17954–17961.
20. Son, Y.-W.; Cohen, M. L.; Louie, S. G. Energy Gaps in Graphene Nanoribbons. *Phys. Rev. Lett.* **2006**, *97*, 216803.
21. Barone, V.; Hod, O.; Scuseria, G. E. Electronic Structure and Stability of Semiconducting Graphene Nanoribbons. *Nano Lett.* **2006**, *6*, 2748–2754.
22. Li, T. C.; Lu, S.-P. Quantum Conductance of Graphene Nanoribbons with Edge Defects. *Phys. Rev. B* **2008**, *77*, 085408.
23. Sols, F.; Guinea, F.; Castro Neto, A. H. Coulomb Blockade in Graphene Nanoribbons. *Phys. Rev. Lett.* **2007**, *99*, 166803.
24. Han, M. Y.; Ozyilmaz, B.; Zhang, Y.; Kim, P. Energy Band-Gap Engineering of Graphene Nanoribbons. *Phys. Rev. Lett.* **2007**, *98*, 206805.
25. Ozyilmaz, B.; Jarillo-Herrero, P.; Efetov, D.; Kim, P. Electronic Transport in Locally Gated Graphene Nanoconstrictions. *Appl. Phys. Lett.* **2007**, *91*, 192107.
26. Chen, Z. H.; Lin, Y.-M.; Rookes, M. J.; Avouris, P. Graphene Nano-Ribbon Electronics. *Phys. E* **2007**, *40*, 228–232.
27. Li, X. L.; Wang, X. R.; Zhang, L.; Lee, S.; Dai, H. J. Chemically Derived Ultrasmooth Graphene Nanoribbon Semiconductors. *Science* **2008**, *319*, 1229–1232.
28. Kosynkin, D. V.; Higginbotham, A. L.; Sinitskii, A.; Lomeda, J. R.; Dimiev, A.; Price, B. K.; Tour, J. M. Longitudinal Unzipping of Carbon Nanotubes to Form Graphene Nanoribbons. *Nature* **2009**, *459*, 872–876.
29. Jiao, L. Y.; Zhang, L.; Wang, X. R.; Diankov, G.; Dai, H. J. Narrow Graphene Nanoribbons From Carbon Nanotubes. *Nature* **2009**, *458*, 877–880.
30. Bai, J.; Duan, X.; Huang, Y. Rational Fabrication of Graphene Nanoribbons Using a Nanowire Etch Mask. *Nano Lett.* **2009**, *9*, 2083–2087.
31. Wei, D.; Liu, Y.; Wang, Y.; Zhang, H.; Huang, L.; Yu, G. Synthesis of N-Doped Graphene by Chemical Vapor Deposition and Its Electrical Properties. *Nano Lett.* **2009**, *9*, 1752–1758.
32. Berashevich, J.; Chakraborty, T. Tunable Band Gap and Magnetic Ordering by Adsorption of Molecules on Graphene. *Phys. Rev. B* **2009**, *80*, 033404.
33. Bai, J.; Zhong, X.; Jiang, S.; Huang, Y.; Duan, X. Graphene Nanomesh. *Nat. Nanotechnol.* **2010**, *5*, 190–194.
34. Cote, L. J.; Cruz-Silva, R.; Huang, J. Flash Reduction and Patterning of Graphite Oxide and Its Polymer Composite. *J. Am. Chem. Soc.* **2009**, *131*, 11027–11032.
35. Williams, G.; Seger, B.; Kamat, P. V. TiO_2-Graphene Nanocomposites. UV-Assisted Photocatalytic Reduction of Graphene Oxide. *ACS Nano* **2008**, *2*, 1487–1491.
36. Akhavan, O.; Ghaderi, E. Photocatalytic Reduction of Graphene Oxide Nanosheets on TiO_2 Thin Film for Photoinactivation of Bacteria in Solar Light Irradiation. *J. Phys. Chem. C* **2009**, *113*, 20214–20220.
37. Li, Z.; Zhang, W.; Luo, Y.; Yang, J.; Hou, J. G. How Graphene Is Cut Upon Oxidation. *J. Am. Chem. Soc.* **2009**, *131*, 6320–6321.
38. Gaya, U. I.; Abdullah, A. H. Heterogeneous Photocatalytic Degradation of Organic Contaminants over Titanium Dioxide: A Review of Fundamentals, Progress and Problems. *J. Photochem. Photobiol., C* **2008**, *9*, 1–12.
39. Kuo, T.-J.; Lin, C.-N.; Kuo, C.-L.; Huang, M. H. Growth of Ultralong ZnO Nanowires on Silicon Substrates by Vapor Transport and Their Use as Recyclable Photocatalysts. *Chem. Mater.* **2007**, *19*, 5143–5147.
40. Tam, K. H.; Djuriši, A. B.; Chan, C. M. N.; Xi, Y. Y.; Tse, C. W.; Leung, Y. H.; Chan, W. K.; Leung, F. C. C.; Au, D. W. T. Antibacterial Activity of ZnO Nanorods Prepared by a Hydrothermal Method. *Thin Solid Films* **2008**, *516*, 6167–6174.
41. Akhavan, O.; Mehrabian, M.; Mirabbaszadeh, K.; Azimirad, R. Hydrothermal Synthesis of ZnO Nanorod Arrays for Photocatalytic Inactivation of Bacteria. *J. Phys. D: Appl. Phys.* **2009**, *42*, 225305.
42. Schniepp, H. C.; Li, J. L.; McAllister, M. J.; Sai, H.; Herrera-Alonso, M.; Adamson, D. H.; Pruïhomme, R. K.; Car, R.; Saville, D. A.; Aksay, I. A. Functionalized Single Graphene Sheets Derived from Splitting Graphite Oxide. *J. Phys. Chem. B* **2006**, *110*, 8535–8539.
43. McAllister, M. J.; Li, J. L.; Adamson, D. H.; Schniepp, H. C.; Abdala, A. A.; Liu, J.; Herrera-Alonso, M.; Milius, D. L.; Car, R.; Pruïhomme, R. K.; Aksay, I. A. Single Sheet Functionalized Graphene by Oxidation and Thermal Expansion of Graphite. *Chem. Mater.* **2007**, *19*, 4396–4404.
44. Yang, D.; Velamakanni, A.; Bozoklu, G.; Park, S.; Stoller, M.; Piner, R. D.; Stankovich, S.; Jung, I.; Field, D. A.; Ventrice, C. A., Jr.; Ruoff, R. S. Chemical Analysis of Graphene Oxide Films after Heat and Chemical Treatments by X-Ray Photoelectron and Micro-Raman Spectroscopy. *Carbon* **2009**, *47*, 145–152.
45. Chiang, T. C.; Seitz, F. Photoemission Spectroscopy in Solids. *Ann. Phys.* **2001**, *10*, 61–74.
46. Yumitori, S. Correlation of C1s Chemical State Intensities with the O1s Intensity in the XPS Analysis of Anodically Oxidized Glass-Like Carbon Samples. *J. Mater. Sci.* **2000**, *35*, 139–146.
47. Kozlowski, C.; Sherwood, P. M. A. X-Ray Photoelectron Spectroscopic Studies of Carbon-Fiber Surfaces. Part 4. The Effect of Electrochemical Treatment in Nitric Acid. *J. Chem. Soc., Faraday Trans. 1* **1984**, *80*, 2099–2107.
48. Tuinstra, F.; Koenig, J. L. Raman Spectrum of Graphite. *J. Chem. Phys.* **1970**, *53*, 1126–1130.
49. Ferrari, A. C.; Robertson, J. Interpretation of Raman Spectra of Disordered and Amorphous Carbon. *Phys. Rev. B* **2000**, *61*, 14095–14107.
50. Graf, D.; Molitor, F.; Ensslin, K.; Stampfer, C.; Jungen, A.; Hierold, C.; Wirtz, L. Spatially Resolved Raman Spectroscopy of Single- and Few-Layer Graphene. *Nano Lett.* **2007**, *7*, 238–242.
51. Kudin, K. N.; Ozbas, B.; Schniepp, H. C.; Pruïhomme, R. K.; Aksay, I. A.; Car, R. Raman Spectra of Graphite Oxide and Functionalized Graphene Sheets. *Nano Lett.* **2008**, *8*, 36–41.
52. Dato, A.; Radmilovic, V.; Lee, Z.; Phillips, J.; Frenkach, M. Substrate Free Gas-Phase Synthesis of Graphene Sheets. *Nano Lett.* **2008**, *8*, 2012–2016.
53. Ferrari, A. C.; Meyer, J. C.; Scardaci, V.; Casiraghi, C.; Lazzeri, M.; Mauri, F.; Piscanec, S.; Jiang, D.; Novoselov, K. S.; Roth, S.; Geim, A. K. The Raman Fingerprint of Graphene and Graphene Layers. *Phys. Rev. Lett.* **2006**, *97*, 187401.
54. Calizo, I.; Balandin, A. A.; Bao, W.; Miao, F.; Lau, C. N. Temperature Dependence of the Raman Spectra of Graphene and Graphene Multilayers. *Nano Lett.* **2007**, *7*, 2645–2649.
55. Akhavan, O. The Effect of Heat Treatment on Formation of Graphene Thin Films from Graphene Oxide Nanosheets. *Carbon* **2009**, *48*, 509–519.
56. Akhavan, O.; Azimirad, R.; Moshfegh, A. Z. Self-Encapsulation of Single-Texture $CoSi_2$ Nanolayer by $TaSi_2$. *Thin Solid Films* **2008**, *516*, 6008–6012.
57. Hummers, W. S.; Offeman, R. E. Preparation of Graphitic Oxide. *J. Am. Chem. Soc.* **1958**, *80*, 1339.